Low photolability of yedoma permafrost dissolved organic carbon

Aron Stubbins[1], Paul J. Mann[2], Leanne Powers[1], Thais B. Bittar[1], Thorsten Dittmar[3], Cameron McIntyre[4,5,6], Timothy I. Eglinton[4], Nikita Zimov[7], Robert G. M. Spencer[8]

[1]Skidaway Institute of Oceanography, Department of Marine Sciences, University of Georgia, 10 Ocean Science Circle, Savannah, GA 31411, USA.

[2]Department of Geography, Northumbria University, Newcastle upon Tyne, NE1 8ST, UK.

[3]Institute for Chemistry and Biology of the Marine Environment, Carl von Ossietzky University Oldenburg, 29129 Oldenburg, Germany.

[4]Geological Institute, Department of Earth Sciences, ETH Zürich, 8092 Zürich, Switzerland.

[5]Laboratory for Ion Beam Physics, Department of Physics, ETH Zürich, 8093 Zürich, Switzerland.

[6]Scottish Universities Environmental Research Centre, East Kilbride, G46 7LS, UK.

[7]Northeast Science Station, Pacific Institute for Geography, Far-Eastern Branch of Russian Academy of Science, Cherskiy, Republic of Sakha (Yakutia), Russia.

[8]Department of Earth, Ocean and Atmospheric Science, Florida State University, Tallahassee, FL 32306, USA.

Corresponding author: Aron Stubbins (aron.stubbins@skio.uga.edu) and Robert G. M. Spencer (rgspencer@fsu.edu)

Key Points:

- Ancient DOC is released from thawing permafrost soils into arctic rivers
- Sunlight preferentially photomineralizes modern arctic river DOC leaving behind ancient permafrost DOC
- Undetectable photochemical losses of permafrost DOC were accompanied by notable photomodification of DOM optical and molecular signatures

Abstract

Vast stores of arctic permafrost carbon that have remained frozen for millennia are thawing, releasing ancient dissolved organic carbon (DOC) to arctic inland waters. Once in arctic waters, DOC can be converted to CO_2 and emitted to the atmosphere, accelerating climate change. Sunlight-driven photoreactions oxidize DOC, converting a portion to CO_2 and leaving behind a photomodified pool of dissolved organic matter (DOM). Samples from the Kolyma River, its tributaries, and streams draining thawing yedoma permafrost were collected. Irradiation experiments and radiocarbon dating were employed to assess the photolability of ancient permafrost-DOC in natural and laboratory generated samples containing a mix of modern and ancient DOC. Photolabile DOC was always modern, with no measurable photochemical loss of ancient permafrost-DOC. However, optical and ultrahigh resolution mass spectrometric measurements revealed that both modern river DOM and ancient permafrost-DOM were photomodified during the irradiations, converting aromatic compounds to less conjugated compounds. These findings suggest that although sunlight-driven photoreactions do not directly mineralize permafrost-DOC, photomodification of permafrost-DOM chemistry may influence its fate and ecological functions in aquatic systems.

1 Introduction

Interactions between anthropogenic climate forcing and natural biogeochemical cycles have the potential to either offset or amplify global change. Amplification occurs via positive feedbacks, for example when an increase in atmospheric CO_2 drives the release of further carbon from vulnerable stores [*Gruber et al.*, 2004]. Arctic permafrost, ground that has been frozen for millennia, holds the largest of these vulnerable global organic carbon (OC) stores (1,100 to 1,700 Pg; 1 Pg = one billion metric tons) [*Schuur et al.*, 2015; *Tarnocai et al.*, 2009]. By 2100, permafrost thaw is projected to release 41 to 288 Pg of this ancient permafrost OC [*Schuur et al.*, 2015]. For comparison, current climate change has been driven by the accumulation of ~250 Pg-C in the present-day atmosphere (based upon an atmospheric CO_2 abundance of ~400 ppm) [*www.esrl.noaa.gov/gmd/ccgg/trends/*]. Although it is clear that permafrost OC is vulnerable, to amplify climate change, permafrost OC needs to be converted to greenhouse gases (e.g. CO_2, methane) [*Schuur et al.*, 2015; *Vonk and Gustafsson*, 2013] and emitted to the atmosphere. As permafrost thaws, a portion of the OC released enters aquatic ecosystems as DOC where it can be rapidly converted to CO_2 by bacterial respiration [*Mann et al.*, 2015; *Spencer et al.*, 2015; *Vonk et al.*, 2013; *Ward and Cory*, 2015] and outgassed efficiently from inland waters [*Vonk and Gustafsson*, 2013].

DOC can also be converted to CO_2 by sunlight-driven photoreactions [*Mopper et al.*, 2015; *Osburn et al.*, 2009]. Recent work reported that photochemistry controls the water column processing of DOC in arctic freshwaters and suggested that photochemistry controls the fate of permafrost-derived DOC [*Cory et al.*, 2014]. Further studies report that DOC from permafrost soils in Alaska is photoreactive [*Ward and Cory*, 2016]. Both the amount of permafrost-derived DOC and solar irradiance received by arctic freshwaters are increasing, the latter due to declining ice cover and expansion of thermokarst lakes [*Surdu et al.*, 2014; *Williamson et al.*, 2014]. Consequently, the photochemical conversion of ancient permafrost DOC to CO_2 may also increase as the Arctic warms. Improved knowledge concerning the photoreactivity of permafrost DOC is therefore critical to predicting the fate of this climate vulnerable ancient carbon and its potential contribution to future global change.

To expand upon previous permafrost DOC photochemical studies that have solely focused on sites in Alaska, samples were collected from the Kolyma River Basin, the sixth largest watershed in the Arctic (~650,000 km^2) and the largest watershed on Earth completely underlain by continuous permafrost [*Spencer et al.*, 2015]. The majority of the permafrost underlying the Kolyma River Basin is Pleistocene-aged yedoma, an organic-rich (1–5% C by mass) permafrost [*Zimov et al.*, 2006]. Yedoma is of singular importance to the strength of carbon-permafrost thaw feedbacks with estimates suggesting between a third to one half of all permafrost OC is stored in yedoma (500 Pg-C) [*Zimov et al.*, 2006]. DOC within yedoma permafrost thaw water streams in the Kolyma River Basin is typically ≥20,000 years old [*Mann et al.*, 2015; *Spencer et al.*, 2015; *Vonk et al.*, 2013], while DOC in the larger streams and rivers of the Kolyma River Basin is predominantly modern [*Mann et al.*, 2015; *Neff et al.*, 2006], presumably due to inputs of DOC from vegetation and surface soils. In a subversion of standard age-bioreactivity relationships, where younger material is expected to be more biolabile [*Raymond and Bauer*, 2001], the ancient permafrost-derived DOC from this region is highly biolabile (>50%) compared to the modern DOC (<10%) in the Kolyma River mainstem [*Spencer et al.*, 2015].

In this study, we determined whether ancient, yedoma permafrost-derived DOC is degraded by sunlight in the absence of microbes. To do this, we collected freshwaters from the same sites within the Kolyma River Basin that were sampled by Spencer et al. [2015]. These sites included a yedoma permafrost thaw stream (Duvanni Yar), small streams (Y3, Y4), a large tributary (Pantileikha River), and the Kolyma River mainstem (Table 1). We sterile filtered and irradiated the samples under a solar simulator for 30 days. We report and discuss the concentration and radiocarbon age of initial and photolabile DOC, along with colored dissolved organic matter (CDOM) light absorbance and ultra-high resolution mass spectrometry data of initial and photomodified DOM.

2 Materials and Methods

2.1 Sample Handling

Fieldwork was conducted out of the Northeast Science Station, Cherskiy, Russia (Fig. 1). Water samples were collected from five sites (Table 1) in September (2014), when annual maxima in permafrost thaw and active layer depth occur [*Spencer et al.*, 2015]. Samples (2 L) were collected in precleaned (acid soaked and ultrapure water rinsed) high-density polyethylene plasticware and kept on ice and in the dark until return to the laboratory (<6 hours) where they were filtered through pre-cleaned (acid soaked, ultrapure water rinsed, and sample flushed) 0.2 μm capsule filters (Whatman Polycap TC) to remove particulates before freezing. Samples were returned frozen to the Skidaway Institute of Oceanography, Savannah, Georgia, USA (~24 hour transit time). Once at Skidaway, samples were transferred to -20°C freezers and stored in the dark until the photochemical experiments were conducted (January 2015).

2.2 Photochemical Experimental Details

Samples were thawed at the Skidaway Institute of Oceanography and refiltered through 0.2 μm GHP syringe filters (Acrodisc). Dissolved organic carbon (DOC) concentrations were determined for all samples. For the photochemical experiments, the permafrost thaw water stream sample was diluted from a concentration of 98.7 mg-C L^{-1} to 3.0 mg-C L^{-1} to prevent the

possibility of high photochemical oxygen demand and other non-photochemical artefacts (e.g. precipitation) that could have occurred at such elevated DOC concentrations. All other samples were irradiated at natural DOC concentrations (Table 1). In addition to irradiating natural waters, approximately carbon-normalized mixtures of yedoma permafrost thaw water and Kolyma River mainstem water were produced generating a series of samples with varying ratios of modern and ancient DOC (Table 2). Aliquots of natural waters and the mixtures were transferred to 100 mL pre-combusted, UV-C sterilized spherical quartz irradiation flasks.

The current study did not seek to quantify real world rates of photoreactions. To determine environmentally relevant rates, spectrally-resolved irradiations and a careful accounting of wavelength specific absorbed photon doses are required to determine the apparent quantum yield spectra that are the starting point for photochemical models [*Hu et al.*, 2002; *Powers et al.*, 2016; *Stubbins et al.*, 2011; *Stubbins et al.*, 2006]. The current study was instead designed to determine the fraction of DOM that is susceptible to photodegradation (i.e. the photolabile fraction) under broadband simulated sunlight [*Stubbins and Dittmar*, 2015; *Stubbins et al.*, 2010]. The broadband irradiation source was a solar simulator fitted with 12 UVA-340 bulbs (Q-Panel), which provide non-collimated light with a spectral shape and flux closely approximating natural sunlight from 295 to 365 nm [*Stubbins et al.*, 2008], the main wavelength range for environmental photochemical reactions involving CDOM [*Mopper et al.*, 2015]. The integrated irradiance quantified in the solar simulator was ~14.4±0.7 W m^{-2} as determined using a spectroradiometer (OL756, Optronic Laboratories) fitted with a quartz fiber optic cable and 2" diameter integrating sphere and calibrated with a NIST standard lamp (OL752-10 irradiance standard) [*Powers and Miller*, 2015].

Absorbance (A) at wavelength λ within the flasks is calculated as:

$$A_{(\lambda)} = a_{(\lambda)} \div 2.303 \times \text{pathlength} \quad (1)$$

where *a* is the Napierian light absorption coefficient (m^{-1}) of CDOM at wavelength λ (nm) and pathlength is the optical pathlength through the flask (m). Percentage transmission (%T) at wavelength λ is then calculated as:

$$\%T_{(\lambda)} = 10^{(2-A_{(\lambda)})} \quad (2)$$

For our study, the outer diameter of the flasks was ~6 cm and inner diameter ~5.5 cm, the discrepancy being due to the thickness of the flasks' quartz walls. The inner diameter determines the pathlength that light will travel through the sample once the flasks are filled. Even with this information, calculating the average pathlength of a sphere within which liquid sample is placed is non-trivial due to variability in the amount of light reflected, which is dependent upon the angle of incidence [*Bolton*, 2000], variation in the pathlength through the sphere due to refraction of light as it travels from air, through the curved quartz surface and into the water, which is dependent upon wavelength and the angle of incidence [*Bolton*, 2000], and the additional uncertainties due to the variable angles of incidence that result from the use of a non-collimated light source. Consequentially, careful and arduous actinometrical tests would have been required

to determine wavelength specific average pathlengths for our spherical flasks and even then, estimates of photon flux and pathlength would have included uncertainties. Keeping these caveats in mind, it is possible to estimate whether the samples placed within the flasks were optically thin for given wavelengths over the range of pathlengths light can travel through the flasks. The following considerations are for 320 nm, a wavelength that absorbed light under the solar simulator and was efficiently photobleached (94 to 98% loss; Table 1). At the start of the experiment, samples ranged in Naperian light absorption coefficient from 3.5 to 74 m^{-1} at 320 nm (Table 1). Assuming that 5.5 cm is the maximum pathlength that light can take through the spherical irradiation flask, this equates to absorbance values (A; optical densities) ranging from 0.08 to 1.8. At this maximum pathlength, none of the samples were optically thin (<90% of light was transmitted) at 320 nm with %T ranging from 82.5 for permafrost thaw water to 1.7 for Y3. The shortest pathlength through the sphere is approximately zero cm and at this pathlength all samples were optically thin. As the irradiation progressed, all samples photobleached, reducing light absorbance and increasing transmission. As the experiments were designed to mimic near-total photobleaching, by the end of the experiment, all samples were optically thin at 320 nm (>90%T for the maximum possible pathlength of 5.5 cm).

The samples were irradiated between 25°C and 30°C. One day of irradiation using this solar simulator is approximate to 18 hours of solar irradiance during July at the Cherskiy field station based upon irradiance modeled using the System for Transfer of Atmospheric Radiation (STAR) [*Ruggaber et al.*, 1994]. Every three days the flasks were swirled to mix the sample and switched between fixed points to account for any variation in the light flux under the solar simulator. For the permafrost and Kolyma River samples, a further four 100 mL flasks were filled and irradiated to allow a time series of CDOM photobleaching to be recorded. This time series allowed photobleaching to be tracked through the experiment until ≥94% of CDOM absorbance at 320 nm was lost. After 30 days of irradiation, ≥94% of CDOM absorbance at 320 nm was lost for all samples and samples were sub-sampled with a pre-combusted Pasteur pipette for analysis of DOC concentration (collected in pre-combusted glass vials and immediately acidified to pH 2 with hydrochloric acid), CDOM (refrigerated in pre-combusted glassware), radiocarbon (frozen in pre-cleaned polycarbonate bottles), and ultrahigh resolution Fourier transform ion cyclotron mass spectrometry (FT-ICR MS; frozen in pre-cleaned polycarbonate bottles).

2.3 Assessment of Potential Microbial Contamination in Photochemical Experiments

Permafrost thaw water DOC from our sampling site is highly biolabile [*Drake et al.*, 2015; *Mann et al.*, 2015; *Spencer et al.*, 2015; *Vonk et al.*, 2013]. Permafrost thaw DOC at other sites in the Arctic, for instance in Alaska, has also been found to be highly biolabile [*Abbott et al.*, 2014; *Ward and Cory*, 2015]. However, previous studies of permafrost-derived DOC photolability have not sterile filtered samples (i.e. they used 0.7 μm GF/F filters) [*Cory et al.*, 2014; *Ward and Cory*, 2016], leaving uncertainty about the direct photolability of permafrost thaw DOC. Therefore, extra care was taken to ensure that the light irradiation experiments in the current study detailed only photochemical effects and not combined photo+bio effects as might be expected if samples were not sterile. Samples were 0.2 μm filtered immediately prior to irradiations to minimize the possibility of microbial contamination. Prior to filling with sample, glassware was also sterilized under UV-C light in a laminar flow hood. Filling of the glassware with samples was conducted in the laminar flow hood with the UV light turned off.

To ascertain whether these precautions were effective in preventing microbial contamination, samples were collected at the end of the photochemical experiments and analyzed for bacterial abundance using flow cytometry. Samples for flow cytometry were preserved with 0.1% glutaraldehyde solution (final concentration) and frozen at -80°C. Ultrapure water and 0.2 µm-filtered sample were run as blanks. Samples were vortexed, and stained for 30 min with Sybr Green I (Thermo Fisher Scientific), a nucleic acid (NA) binding stain [*Marie et al.*, 1997]. Bacterial cells were counted using a flow cytometer (BD FACSCalibur) equipped with a 15 mW air-cooled argon-ion laser tuned for blue excitation (ex 488 nm), with emission (em) detectors at 535, 585 and 650 nm. Runs were calibrated with fluorescent polystyrene beads (1 µm, Spherotech) added to each sample to ensure instrument reproducibility and provide a fluorescence reference. Data were acquired using BD Cell Quest Pro software (v. 4.0.1) and analyzed with FlowJo software (v.10).

Counts in samples (Table 3) were below those of the ultrapure water (10 counts) and Sample Blank (66 counts) in all samples except Y3. Blank counts reflect background noise. The counts recorded for Y3 are still within the typical range for river water blanks (0.2 µm filtered samples; e.g., 7 to 758 counts for samples from the Connecticut River Basin run on the same instrument and using the same settings in the same month. River Water Blank Counts Mean = 212; n = 24). Based upon this data, we conclude that all samples were sterile. Of major significance are the extremely low counts (count = 2; Table 3) observed for the highly biolabile, 100% permafrost thaw sample, indicating that this sample was sterile, as were the other mixtures in the photo-priming experiment (Table 3). These results add confidence to our assertion that our experiments assessed the direct photolability of permafrost thaw DOC in the absence of biological artifacts.

2.4 Quantification of Dissolved Organic Carbon

Samples acidified to pH 2 by addition of hydrochloric acid (p.a.) were analyzed for non-purgable organic carbon using a Shimadzu TOC-V_{CPH} analyzer fitted with a Shimadzu ASI-V autosampler. Potassium hydrogen phthalate standards were analyzed. In addition to standards, aliquots of deep seawater reference material, Batch 10, Lot# 05-10, from the Consensus Reference Material Project (CRM) were analyzed to check the precision and accuracy of the DOC analyses. Analyses of the CRM deviated by less than 5% from the reported value for these standards (41 to 44 µM-DOC) [*http://yyy.rsmas.miami.edu/groups/biogeochem/Table1.htm*]. Routine minimum detection limits in the investigator's laboratory using the above configuration are 34±4 µg-C and standard errors are typically 1.7±0.5 % of the DOC concentration [*Stubbins and Dittmar*, 2012]. The photolabile fraction of DOC (DOC_{photo}) was calculated as:

$$DOC_{photo} = DOC_{initial} - DOC_{final} \quad (3)$$

where $DOC_{initial}$ is the concentration of DOC in the initial samples and DOC_{final} is the DOC concentration in the samples after 30 days of irradiation. Percentage DOC_{photo} was then calculated as DOC_{photo} divided by $DOC_{initial}$ multiplied by 100.

2.5 Stable and Radiocarbon Analysis

$\delta^{13}C$ analyses were conducted at the University of California, Davis Stable Isotope Facility and ^{14}C analyses at the Laboratory for Ion Beam Physics, Eidgenossiche Technische Hochschule (ETH) Zürich. $\delta^{13}C$-DOC samples were analyzed using an O.I. Analytical Model 1010 TOC analyzer (precision of ±0.2%) interfaced to a PDZ Europa 20–20 IRMS (Sercon Ltd). $\delta^{13}C$-DOC measurements were calibrated against the $\delta^{13}C$ values of KHP and IHSS Suwannee River humic acid in ultrapure water. Waters for ^{14}C-DOC analyses were freeze-dried (Christ Alpha 2-4, LSC with a low-carbon vacuum hybrid pump, Vacubrand RC-6; Martin Christ, Labex Instrument AB, Sweden) directly in pre-combusted (850°C/5 h) quartz tubes. Samples were fumigated with hydrochloric acid for 24 hrs at 60°C to remove carbonates and flame sealed with pre-combusted CuO under vacuum. CO_2 gas was cryogenically captured and quantified (~30 μg-C) before measurement using an accelerator mass spectrometer (AMS) fitted with a gas accepting ion source (MICADAS, Ionplus AG) [*Mann et al.*, 2015]. Combusted NIST SRM 4990C oxalic acid was used as a standard for normalization, and blanks were determined using radiocarbon-free CO_2, both at a concentration of 5% CO_2 in He. The modern oxalic acid standard was measured to 3 ‰ relative error and the blank value was 39,400 (years before present, yBP). Samples were run until they were fully consumed giving relative errors of 1-4%.

Radiocarbon contents are reported as fraction modern ($F^{14}C$) and ^{14}C age (yBP) [*Reimer et al.*, 2004; *Stenström et al.*, 2011]. All radiocarbon values were corrected for a procedural blank (0.6 μg-C; $F^{14}C$ of 0.3 ± 0.1). The apparent ^{14}C age of the photolabile DOC fraction ($[DOC]_{photo}$) was calculated using measurements of initial DOC ($[DOC]_{initial}$) and final DOC concentrations ($[DOC]_{final}$) alongside the associated change in isotopic composition using a simple mass balance:

$$[\mathrm{DOC}]_{\mathrm{photo}} \times \mathrm{F^{14}C_{photo}} = [\mathrm{DOC}]_{\mathrm{initial}} \times \mathrm{F^{14}C_{initial}} - [\mathrm{DOC}]_{\mathrm{final}} \times \mathrm{F^{14}C_{final}} \quad (4)$$

Individual errors associated with DOC concentration and isotope measurements were propagated to assess error on $F^{14}C_{photo}$ and apparent age of the photolabile DOC (Table 1 and 3). A paired t-test was used to assess the statistical significance of the change in fraction modern ($F^{14}C$) between the initial and final sample means.

2.6 Spectrophotometric Analysis of Colored Dissolved Organic Matter

Following irradiation, aliquots were transferred from the flasks to combusted glass vials, which were then capped with Teflon septa and placed in the dark for approximately 8 hours in order to return to room temperature. Subsequently, each aliquot was transferred to a 1 cm quartz absorbance cuvette (Starna Cells) using a pre-combusted Pasteur pipette. The cuvette was then situated in the light path of an Agilent 8453 ultraviolet-visible spectrophotometer and a sample CDOM absorbance spectrum was recorded. An aliquot of temperature equilibrated ultrapure water was run immediately before and after the samples, as well as every ~10 samples, to provide a blank. Blank corrected absorbance spectra were then corrected for offsets due to scattering and instrument drift by subtraction of the average absorbance between 700 and 800 nm [*Stubbins et al.*, 2011]. Data output from the spectrophotometer were in the form of dimensionless absorbance (A) and were converted to the Napierian absorption coefficient, *a* (m^{-1}) [*Hu et al.*, 2002]. The percentage loss of *a* at 320 and 254 nm was calculated:

$$\%\ \text{Photolabile}\ a_{(\lambda)} = \left(\text{Initial}\ a_{(\lambda)} - \text{Final}\ a_{(\lambda)}\right) \div \text{Initial}\ a_{(\lambda)} \times 100 \quad (5)$$

The carbon-normalized light absorbance at 254 nm ($SUVA_{254}$; L mg-C^{-1} m^{-1}) was then calculated by dividing the Decadic light absorption coefficient at 254 nm (m^{-1}; i.e. the Napierian absorption coefficient / 2.303) by the DOC concentration (mg-C L^{-1}) [*Weishaar et al.*, 2003]. This calculation was performed for the initial and photodegraded DOM samples, and for the fraction of DOC and CDOM absorbance lost during irradiation. Individual errors associated with DOC concentration and absorbance measurements were propagated to assess error in the apparent $SUVA_{254}$ of photolabile DOC (DOC_{photo} in Table 1).

2.7 Fourier Transform Ion Cyclotron Mass Spectrometry

Samples were analyzed via ultrahigh resolution FT-ICR MS without prior extraction or isolation, allowing the broadest possible analytical window for electrospray ionization FT-ICR MS. Samples were diluted 1:1 with ultrapure water and analyzed in negative mode electrospray ionization using a 15 Tesla FT-ICR MS (Bruker Solarix) at the University of Oldenburg, Germany [*Spencer et al.*, 2015]. 500 broadband scans were accumulated for the mass spectra. After internal calibration, mass accuracies were within an error of <0.2 ppm. Molecular formulas were assigned to detected masses with signal to noise ratios greater than five, based on published rules [*Singer et al.*, 2012; *Stubbins et al.*, 2010]. Compounds detected in the procedural blank (ultrapure water) were removed. Detection limits were standardized between samples by adjusting the dynamic range of each sample to that of the sample with the lowest dynamic range (dynamic range = average of the largest 20% of peaks assigned a formula divided by the signal to noise threshold intensity; standardized detection limit = average of largest 20% of peaks assigned a formula within a sample divided by the lowest dynamic range within the sample set) [*Stubbins et al.*, 2014]. Peaks below this detection limit were removed to prevent false negatives for the occurrence of a formula within samples with low dynamic range.

For each molecular formula, we calculated the modified Aromaticity Index (AI_{mod}) [*Koch and Dittmar*, 2006; 2016], which indicates the likelihood of a molecular formula representing aromatic structures, from an AI_{mod} of zero, where formulas are aliphatic, through an intermediate range, where a molecular formula could indicate aromatic or non-aromatic isomers, to AI_{mod} values above 0.5, where a molecular formula is highly likely to represent aromatic isomers [*Koch and Dittmar*, 2006]. These AI_{mod} values were calculated as:

$$AI_{mod} = (1 + C - 0.5O - S - 0.5(N+P+H)) \,/\, (C - 0.5O - S - N - P) \quad (5)$$

The main goal of the FT-ICR MS analyses in the current study was to determine the molecular signatures of photomodification. In order to do this, FT-ICR MS formulas were classified as photolabile (>30% reduction in peak intensity), photoproduced (>30% increase in peak intensity), and photorefractory (<30% change in peak intensity). The choice of the percentage change in normalized signal intensity (i.e. 30%) is somewhat arbitrary. However, similar molecular trends were apparent when different percentages were utilized, indicating that the inferences made with the choice of 30% differences represent robust trends in molecular photomodification. In defining these groupings, it should be remembered that electrospray ionization is selective, and that this selectivity results in one peak's intensity changing relative to

increases or decreases in other peak intensities. Therefore, a molecular formula that appeared to be produced during the irradiation may have been present in the sample all along, but emerged from the background as other peaks were removed during photodegradation. Alternatively, a molecular formula identified as labile, may also still be present at the end of the experiment, but may not show up if photoproducts with high ionization efficiencies are photoproduced.

3 Results and Discussion

3.1 Photostability of Ancient, Yedoma Permafrost-derived DOC

The DOC in yedoma permafrost thaw streams was verified as being ancient permafrost-derived DOC (20,000 yBP) and showed no measurable photochemical loss (Table 1). By contrast, irradiation of river samples containing modern DOC resulted in significant DOC losses (26 to 40%; Table 1). These trends in DOC photolability (i.e. percentage DOC loss during photodegradation) contrast with trends in DOC biolability which was much higher in samples from the same permafrost thaw stream (~62% biolabile) than for the Kolyma River (~7% biolabile) [*Spencer et al.*, 2015].

An isotope balance approach (Equation 4) was applied to calculate the apparent age of DOC lost during the irradiations of permafrost thaw stream and other Kolyma River Basin waters. The mean $F^{14}C$ of final samples were significantly lower (older) than initial samples ($t = 2.61$, degrees freedom = 7; $p < 0.05$). $F^{14}C$ values for DOC_{photo} indicated that photolabile DOC was always modern (Table 1). This contrasts with results from biodegradation experiments with waters from the same field sites, where microbes preferentially utilized ancient DOC [*Mann et al.*, 2015; *Spencer et al.*, 2015].

In the current study, samples were irradiated for 30 days under a solar simulator. The areal light dose received was equivalent to approximately 22.5 days of natural solar irradiance at the latitude of the Kolyma River (see methods). This timeframe is approximately equivalent to the transit time of water from the Kolyma River source to the sea [*Holmes et al.*, 2012]. However, the similarity in these timeframes should not be interpreted as a similarity in the light dose received by the irradiated samples and CDOM in the Kolyma River as it is carried toward the ocean. In the river, the water column mixes and the photochemical potency of the solar irradiance dose received and absorbed in the top few centimeters of the surface is effectively diluted throughout the depth of the water column. In our experimental setup, samples received much higher photon doses per unit volume as they were trapped in a spherical flask with a 5.5 cm internal diameter. As the samples in our experiments photobleached, they also became optically thin, increasing the penetration of light into the flask and increasing the photon dose absorbed per unit CDOM. Consequently, the light dose absorbed per unit CDOM over 30 days in our experiments is likely only experienced by Kolyma River CDOM in nature once the CDOM has been exported to and diluted within the coastal ocean. Even at this point, CDOM derived from the Kolyma River would need to remain in low color, stratified waters for many months to receive a photon dose approaching those absorbed by CDOM in our experiments. Furthermore, the permafrost thaw stream sample had the lowest initial absorbance of all the samples collected (Table 1). Therefore, permafrost-DOM received a greater photon dose per unit CDOM than received by the optically thicker river water samples. Based upon these considerations, the stability of permafrost-derived DOC under the unnaturally high photon dose conditions of our

experiments, suggest that permafrost-derived DOC will be highly resistant to photomineralization in natural waters.

The contrasting rapid and preferential loss of ancient permafrost DOC during bio-incubations and undetectable loss of ancient permafrost DOC during photochemical irradiations indicate that microbial processes are likely responsible for the loss of permafrost-derived DOC from arctic freshwaters, at least for permafrost DOC derived from the organic-rich yedoma that is the greatest store of climate-vulnerable ancient permafrost organic carbon [*Zimov et al.*, 2006].

3.2 Dissolved Organic Matter Photomodification

The aromatic molecules comprising the CDOM pool are the primary light absorbing chromophores and initiators of photoreactions in natural waters [*Mopper et al.*, 2015]. The permafrost thaw sample had the lowest carbon-normalized CDOM absorbance ($SUVA_{254}$), a proxy for aromaticity [*Weishaar et al.*, 2003], of the samples studied (Table 1), consistent with previous studies that also report low CDOM absorbance levels for permafrost-derived DOM [*Abbott et al.*, 2014; *Mann et al.*, 2014]. The low $SUVA_{254}$ of permafrost-derived DOM likely partly explains its low photolability. Although permafrost-derived DOC was not significantly photolabile (i.e. DOC loss was below detection limits), 78% of permafrost-derived CDOM was photobleached (Table 1). Consistent with previous studies [*Mopper et al.*, 2015; *Osburn et al.*, 2009; *Spencer et al.*, 2009; *Stubbins et al.*, 2012], CDOM was also preferentially photobleached (78 to 89%) relative to DOC (0 to 40%) in all samples (Table 1). The preferential loss of CDOM relative to DOC during photodegradation resulted in photolabile DOM apparent $SUVA_{254}$ values ranging from 5.7 to 12.2 L mg-C^{-1} m^{-1} (Table 1). These calculated $SUVA_{254}$ values for the organic matter lost during photodegradation exceed the maximum values normally observed in natural waters (~5 L mg-C^{-1} m^{-1}) [*Mann et al.*, 2014; *Spencer et al.*, 2012], indicating that irradiation resulted in the loss of an organic matter pool that was enriched in colored, aromatic moieties.

The molecular signatures accompanying the apparent photomodification of DOM in permafrost thaw and Kolyma mainstem waters were determined by FT-ICR MS [*Dittmar and Stubbins*, 2014]. Molecular formulas were classified as photolabile (>30% reduction in signal intensity), photoproduced (>30% increase in signal intensity), and photorefractory (<30% change in signal intensity). Consistent with previous results for river [*Stubbins et al.*, 2010] and ocean DOM [*Stubbins and Dittmar*, 2015], aromatic formulas (AI_{mod} >0.5) were highly photolabile and aliphatics (AI_{mod} <0.1) were the main photoproducts within both permafrost and Kolyma River DOM (Fig. 2a,b), indicating that the preferential photochemical loss of CDOM is driven by the photomodification of colored aromatic compounds to non-aromatic, transparent DOM. Furthermore, these results suggest that the photobleaching of permafrost CDOM that occurred without significant DOC losses may have been driven by the photo-induced cleavage of aromatic ring structures in CDOM to form non-colored, non-aromatic DOM photoproducts as exemplified by aliphatic compounds.

3.3 Potential Influence of Photomodification upon DOC Biolability

Photomodification can alter DOC biolability. For instance, experiments irradiating low biolability DOC from colored, aromatic-rich freshwaters generally report an increase in DOC biolability after irradiation [*Cory et al.*, 2014; *Miller and Moran*, 1997]; while photodegradation of highly biolabile DOC can decrease its biolability [*Bittar et al.*, 2015]. Thus, for the colored, modern DOM samples irradiated here, it is likely that photomodification increased DOC

biolability as observed for other arctic freshwaters [*Cory et al.*, 2014]. The aliphatic compounds that are enriched in permafrost-derived DOM relative to Kolyma River DOM (AI_{mod} <0.1 Fig. 2a,b; H/C >1.5 Fig. 2C&D) are highly biolabile [*Spencer et al.*, 2015]. These classes of aliphatic compounds were photorefractory or photoproduced in the current experiments (Fig. 2). Therefore, we may expect the photomodification and accompanying photoproduction of aliphatics to also enhance the biolability of permafrost DOC. However, until direct measurements of the enhanced microbial utilization of radiocarbon depleted DOC post-irradiation are made, it remains unclear whether photomodification of highly biolabile permafrost DOC will result in an increase or decrease in its biolability.

3.4 Photochemical Priming

When CDOM absorbs sunlight, secondary photochemical or photosensitization reactions can lead to the indirect photodegradation of organic compounds [*Chin et al.*, 2004]. Consequently, we hypothesized that sunlight absorbed by relatively photolabile, aromatic-rich, modern DOM, could lead to the indirect photomineralization of relatively aromatic-poor, ancient permafrost-derived DOM as the latter mixes into arctic fluvial networks. We term this potential indirect photomineralization "photo-priming".

To test for photo-priming, carbon-normalized mixtures of permafrost thaw and Kolyma River waters were irradiated. The photobleaching of CDOM absorbance, the percentage of photolabile DOC, and the percentage of photolabile molecular formulas all increased linearly with the proportion of Kolyma River DOC in the mixture (Fig. 3a-c). Concurrently, the fraction of modern DOC in each mixture decreased significantly during the irradiations (Fig. 3d; paired t-test (df 7) $t = 2.61$, $p < 0.05$), highlighting that modern DOC was consistently photomineralized. Where the loss of DOC during irradiations was above detection limits (0 to 39% permafrost-derived DOC mixtures), the photomineralized DOC was consistently modern (Table 2) clearly showing that no significant loss of ancient permafrost-derived DOC occurred either through direct photochemical reactions or secondary, photo-priming reactions (Table 2). Thus, yedoma permafrost-derived DOC is unlikely to undergo photomineralization as it mixes into arctic rivers containing modern, colored DOM.

4. Conclusions

Delineating the controls on the fate of thawed permafrost-derived DOC is critical to assessing how the Arctic carbon cycle will impact the aquatic ecosystems of the Arctic and their role in global climate change. Although photochemistry appears to be quantitatively important for the mineralization of modern arctic DOC to CO_2 [*Cory et al.*, 2014], photochemistry does not appear to have a significant, direct influence upon the fate of ancient yedoma permafrost-derived DOC. Due to the high biolability of yedoma permafrost-derived DOC [*Abbott et al.*, 2014; *Drake et al.*, 2015; *Mann et al.*, 2015; *Spencer et al.*, 2015; *Vonk et al.*, 2013], we suggest that microbial activity, rather than sunlight, will control the strength of the positive feedback between climate change, carbon mobilization to inland waters due to yedoma permafrost thaw, and the release of ancient permafrost-derived CO_2 to the atmosphere.

Acknowledgments

This work was supported by University of Georgia, Skidaway Institute of Oceanography research stimulation funds granted to Aron Stubbins and the US National Science Foundation (ANT-1203885/PLR-1500169) to Robert G. M. Spencer. Daniel Montluçon (ETH Zürich) is thanked for assistance and advice with sample preparation for radiocarbon analysis, along with Lukas Wacker and other members of the Laboratory for Ion Beam Physics (ETH Zürich). The data used are listed in the references and tables.

References

Abbott, B. W., J. R. Larouche, J. B. Jones, W. B. Bowden, and A. W. Balser (2014), Elevated dissolved organic carbon biodegradability from thawing and collapsing permafrost, *Journal of Geophysical Research: Biogeosciences*, *119*(10), 2014JG002678.

Bittar, T. B., A. A. Vieira, A. Stubbins, and K. Mopper (2015), Competition between photochemical and biological degradation of dissolved organic matter from the cyanobacteria Microcystis aeruginosa, *Limnology and Oceanography*, *60*(4), 1172-1194.

Bolton, J. R. (2000), Calculation of ultraviolet fluence rate distributions in an annular reactor: significance of refraction and reflection, *Water Research*, *34*(13), 3315-3324.

Chin, Y.-P., P. L. Miller, L. Zeng, K. Cawley, and L. K. Weavers (2004), Photosensitized degradation of bisphenol A by dissolved organic matter, *Environmental Science and Technology*, *38*(22), 5888-5894.

Cory, R. M., C. P. Ward, B. C. Crump, and G. W. Kling (2014), Sunlight controls water column processing of carbon in arctic fresh waters, *Science*, *345*(6199), 925-928.

Dittmar, T., and A. Stubbins (2014), 12.6 - Dissolved Organic Matter in Aquatic Systems A2 - Holland, Heinrich D, in *Treatise on Geochemistry (Second Edition)*, edited by K. K. Turekian, pp. 125-156, Elsevier, Oxford.

Drake, T. W., K. P. Wickland, R. G. Spencer, D. M. McKnight, and R. G. Striegl (2015), Ancient low–molecular-weight organic acids in permafrost fuel rapid carbon dioxide production upon thaw, *Proceedings of the National Academy of Sciences*, *112*(45), 13946-13951.

Gruber, N., P. Friedlingstein, C. B. Field, R. Valentini, M. Heimann, J. E. Richey, P. R. Lankao, E.-D. Schulze, and C.-T. A. Chen (2004), The vulnerability of the carbon cycle in the 21st century: An assessment of carbon-climate-human interactions, in *The Global Carbon Cycle: Integrating Humans, Climate, and the Natural World*, edited by M. R. R. Christopher B. Field, pp. 45-76, Island Press, Washington DC.

Holmes, R. M., et al. (2012), Seasonal and annual fluxes of nutrients and organic matter from large rivers to the Arctic Ocean and surrounding seas, *Estuaries and Coasts*, *35*(2), 369-382.

http://yyy.rsmas.miami.edu/groups/biogeochem/Table1.htm.

Hu, C., F. E. Muller-Karger, and R. G. Zepp (2002), Absorbance, absorption coefficient, and apparent quantum yield: A comment on common ambiguity in the use of these optical concepts, *Limnology and Oceanography*, *47*(4), 1261-1267.

Koch, B. P., and T. Dittmar (2006), From mass to structure: An aromaticity index for high-resolution mass data of natural organic matter, *Rapid Communications in Mass Spectrometry*, *20*(5), 926-932.

Koch, B. P., and T. Dittmar (2016), From mass to structure: an aromaticity index for high-resolution mass data of natural organic matter, *Rapid Communications in Mass Spectrometry*, *30*(1), 250-250.

Mann, P. J., T. I. Eglinton, C. P. McIntyre, N. Zimov, A. Davydova, J. E. Vonk, R. M. Holmes, and R. G. Spencer (2015), Utilization of ancient permafrost carbon in headwaters of Arctic fluvial networks, *Nature Communications*, *6*, 7856.

Mann, P. J., et al. (2014), Evidence for key enzymatic controls on metabolism of Arctic river organic matter, *Global Change Biology*, *20*(4), 1089-1100.

Marie, D., F. Partensky, S. Jacquet, and D. Vaulot (1997), Enumeration and cell cycle analysis of natural populations of marine picoplankton by flow cytometry using the nucleic acid stain SYBR Green I, *Applied and Environmental Microbiology*, *63*(1), 186-193.

Miller, W. L., and M. A. Moran (1997), Interaction of photochemical and microbial processes in the degradation of refractory dissolved organic matter from a coastal marine environment, *Limnology and Oceanography*, *42*(6), 1317-1324.

Mopper, K., D. J. Kieber, and A. Stubbins (2015), Marine photochemistry: Processes and impacts, in *Biogeochemistry of Marine Dissolved Organic Matter*, edited by D. A. Hansell, Carlson, C. A., pp. 389-450, Elsevier.

Neff, J., J. Finlay, S. Zimov, S. Davydov, J. Carrasco, E. Schuur, and A. Davydova (2006), Seasonal changes in the age and structure of dissolved organic carbon in Siberian rivers and streams, *Geophysical Research Letters*, *33*(23).

Osburn, C. L., L. Retamal, and W. F. Vincent (2009), Photoreactivity of chromophoric dissolved organic matter transported by the Mackenzie River to the Beaufort Sea, *Marine Chemistry*, *115*(1), 10-20.

Powers, L. C., and W. L. Miller (2015), Photochemical production of CO and CO 2 in the Northern Gulf of Mexico: Estimates and challenges for quantifying the impact of photochemistry on carbon cycles, *Marine Chemistry*, *171*, 21-35.

Powers, L. C., J. A. Brandes, W. L. Miller, and A. Stubbins (2016), Using liquid chromatography-isotope ratio mass spectrometry to measure the $\delta^{13}C$ of dissolved inorganic carbon photochemically produced from dissolved organic carbon, *Limnology and Oceanography: Methods, doi:10.1002/lom3.10146*.

Raymond, P. A., and J. E. Bauer (2001), Riverine export of aged terrestrial organic matter to the North Atlantic Ocean, *Nature*, *409*(6819), 497-500.

Reimer, P. J., T. A. Brown, and R. W. Reimer (2004), Discussion: reporting and calibration of post-bomb 14C data, *Radiocarbon*, *46*(3), 1299-1304.

Ruggaber, A., R. Dlugi, and T. Nakajima (1994), Modelling radiation quantities and photolysis frequencies in the troposphere, *Journal of Atmospheric Chemistry*, *18*(2), 171-210.

Schuur, E., A. McGuire, C. Schädel, G. Grosse, J. Harden, D. Hayes, G. Hugelius, C. Koven, P. Kuhry, and D. Lawrence (2015), Climate change and the permafrost carbon feedback, *Nature*, *520*(7546), 171-179.

Singer, G. A., C. Fasching, L. Wilhelm, J. Niggemann, P. Steier, T. Dittmar, and T. J. Battin (2012), Biogeochemically diverse organic matter in Alpine glaciers and its downstream fate, *Nature Geoscience*, *5*(10), 710-714.

Spencer, R. G. M., K. D. Butler, and G. R. Aiken (2012), Dissolved organic carbon and chromophoric dissolved organic matter properties of rivers in the USA, *Journal of Geophysical Research: Biogeosciences*, *117*(3).

Spencer, R. G. M., P. J. Mann, T. Dittmar, T. I. Eglinton, C. McIntyre, R. M. Holmes, N. Zimov, and A. Stubbins (2015), Detecting the signature of permafrost thaw in Arctic rivers, *Geophysical Research Letters*, *42*(8), 2830-2835.

Spencer, R. G. M., et al. (2009), Photochemical degradation of dissolved organic matter and dissolved lignin phenols from the Congo River, *Journal of Geophysical Research: Biogeosciences*, *114*, G03010, doi:03010.01029/02009JG000968.

Stenström, K., G. Skog, E. Georgiadou, J. Genberg, and A. Johansson (2011), A guide to radiocarbon units and calculations, *LUNFD6 (NFFR-3111)/1-17/(2011)*.

Stubbins, A., and T. Dittmar (2012), Low volume quantification of dissolved organic carbon and dissolved nitrogen, *Limnology and Oceanography: Methods*, *10*, 347-352.

Stubbins, A., and T. Dittmar (2015), Illuminating the deep: Molecular signatures of photochemical alteration of dissolved organic matter from North Atlantic Deep Water, *Marine Chemistry*, *177*, *Part 2*, 318-324.

Stubbins, A., J. Niggemann, and T. Dittmar (2012), Photo-lability of deep ocean dissolved black carbon, *Biogeosciences*, *9*(5), 1661-1670.

Stubbins, A., C. S. Law, G. Uher, and R. C. Upstill-Goddard (2011), Carbon monoxide apparent quantum yields and photoproduction in the Tyne estuary, *Biogeosciences*, *8*(3), 703-713.

Stubbins, A., G. Uher, C. S. Law, K. Mopper, C. Robinson, and R. C. Upstill-Goddard (2006), Open-ocean carbon monoxide photoproduction, *Deep-Sea Research Part II: Topical Studies in Oceanography*, *53*(14-16), 1695-1705.

Stubbins, A., J. F. Lapierre, M. Berggren, Y. T. Prairie, T. Dittmar, and P. A. del Giorgio (2014), What's in an EEM? Molecular Signatures Associated with Dissolved Organic Fluorescence in Boreal Canada, *Environmental Science and Technology*, *48*(18), 10598-10606.

Stubbins, A., V. Hubbard, G. Uher, C. S. Law, R. C. Upstill-Goddard, G. R. Aiken, and M. Kenneth (2008), Relating carbon monoxide photoproduction to dissolved organic matter functionality, *Environmental Science and Technology*, *42*(9), 3271-3276.

Stubbins, A., R. G. M. Spencer, H. Chen, P. G. Hatcher, K. Mopper, P. J. Hernes, V. L. Mwamba, A. M. Mangangu, J. N. Wabakanghanzi, and J. Six (2010), Illuminated darkness: Molecular signatures of Congo River dissolved organic matter and its photochemical alteration as revealed by ultrahigh precision mass spectrometry, *Limnology and Oceanography*, *55*(4), 1467-1477.

Surdu, C. M., C. R. Duguay, L. C. Brown, and D. Fernández Prieto (2014), Response of ice cover on shallow lakes of the North Slope of Alaska to contemporary climate conditions (1950–2011): radar remote-sensing and numerical modeling data analysis, *The Cryosphere*, *8*(1), 167-180.

Tarnocai, C., J. Canadell, E. Schuur, P. Kuhry, G. Mazhitova, and S. Zimov (2009), Soil organic carbon pools in the northern circumpolar permafrost region, *Global Biogeochemical Cycles*, *23*, GB2023, doi:2010.1029/2008GB003327.

Vonk, J. E., and Ö. Gustafsson (2013), Permafrost-carbon complexities, *Nature Geoscience*, *6*(9), 675-676.

Vonk, J. E., et al. (2013), High biolability of ancient permafrost carbon upon thaw, *Geophysical Research Letters*, *40*(11), 2689-2693.

Ward, C. P., and R. M. Cory (2015), Chemical composition of dissolved organic matter draining permafrost soils, *Geochimica et Cosmochimica Acta*, *167*, 63-79.

Ward, C. P., and R. M. Cory (2016), Complete and partial photo-oxidation of dissolved organic matter draining permafrost soils, *Environmental Science and Technology*, *50*(7), 3545–3553.

Weishaar, J. L., G. R. Aiken, B. A. Bergamaschi, M. S. Fram, R. Fujii, and K. Mopper (2003), Evaluation of specific ultraviolet absorbance as an indicator of the chemical composition and reactivity of dissolved organic carbon, *Environmental Science and Technology*, *37*(20), 4702-4708.

Williamson, C. E., et al. (2014), Solar ultraviolet radiation in a changing climate, *Nature Clim. Change*, *4*(6), 434-441.

www.esrl.noaa.gov/gmd/ccgg/trends/.

Zimov, S. A., E. A. Schuur, and F. S. Chapin III (2006), Permafrost and the global carbon budget, *Science(Washington)*, *312*(5780), 1612-1613.

Table 1 | Initial dissolved organic carbon (DOC) concentration, fraction modern ($F^{14}C$), apparent radiocarbon age in years before present (yBP), colored dissolved organic matter (CDOM) light absorption coefficient at 254 nm (a_{254}), and specific ultraviolet light absorbance of DOM at 254 nm ($SUVA_{254}$) for a permafrost thaw water stream, two small order streams underlain by permafrost (Y3, Y4), a large tributary (Pantileikha River), and the Kolyma River mainstem, all within the Kolyma River Basin, as well as the percentage photolabile DOC (DOC_{photo}) and a_{254}, and the $F^{14}C$, apparent age, and $SUVA_{254}$ of DOC_{photo} that was lost from each sample during 30 days of irradiation in a solar simulator and the decimal degrees latitude and longitude for each site. Modern is defined as $F^{14}C$ that is not significantly different from 1.0.

	Permafrost Thaw* Water Stream	Y3	Y4	Pantileikha River	Kolyma River Mainstem
Latitude:	68.6305:	68.7592:	68.7424:	68.7120:	68.7891:
Longitude	159.1501	161.4477	161.4137	161.4942	161.3132
Initial DOC (mg-C L^{-1})	3.0±0.1	24.4±0.6	21.4±0.7	12.1±0.5	4.8±0.1
% DOC_{photo}	-3±4 %	40±2 %	28±3 %	31±4 %	26±2%
Initial a_{320} (m^{-1})	3.5	74	58	34	11
% Photolabile a_{320}	94 %	98 %	97 %	97 %	98 %
Initial a_{254} (m^{-1})	11	188	151	88	30
% Photolabile a_{254}	78 %	89 %	85 %	87 %	86 %
Initial $SUVA_{254}$ (L mg-C^{-1} m^{-1})	1.7	3.3	3.1	3.1	2.7
$SUVA_{254}$ of DOC_{photo} (L mg-C^{-1} m^{-1})	NA	7.4±0.3	9.3±1.5	8.6±1.2	8.8±0.8
$F^{14}C$ of Initial DOC	0.087±0.01	1.06±0.01	1.05±0.01	1.05±0.01	0.993±0.002
$F^{14}C$ of DOC_{photo}	NA	1.04±0.06	1.0±0.1	1.0±0.1	0.93±0.09
^{14}C Age of Initial DOC	20,000 yBP	Modern	Modern	Modern	Modern
^{14}C Age of DOC_{photo}	NA	Modern	Modern	Modern	Modern

*The permafrost thaw water sample was diluted from 98.7 mg-C L^{-1} to 3.0 mg-C L^{-1} to prevent artifacts that could have occurred at elevated DOC concentrations.

Table 2 | Percentages of dissolved organic carbon (DOC) derived from permafrost thaw water or Kolyma River water and DOC apparent age in years before present (yBP) within Kolyma River water:permafrost thaw stream water mixtures, as well as the percentage, fraction modern ($F^{14}C$) and apparent age of the photolabile DOC (DOC_{photo}) lost during 30 day irradiations in a solar simulator. *DOC loss in mixtures with less than 61% Kolyma River DOC was within analytical error introducing uncertainties into estimates of the $F^{14}C$ and apparent age of DOC_{photo} in these samples. Modern is defined as $F^{14}C$ that is not significantly different from 1.0.

% Permafrost DOC	100%	98%	92%	66%	39%	17%	3%	1%	0%
% Kolyma River DOC	0%	2%	8%	34%	61%	83%	97%	99%	100%
^{14}C Age of Initial DOC	20,000	17,100	12,400	7,380	3,580	1,510	Modern	Modern	Modern
% DOC_{photo}	*-3±4%	*3±3%	*3±4%	*4±3%	14±3%	22±3%	25±3%	27±2%	26±2%
$F^{14}C$ of DOC_{photo}	0.1±0.1	0.9±1.2	1.6±2.2	2.0±1.9	1.1±0.2	0.9±0.1	1.0±0.1	1.0±0.1	0.9±0.1
^{14}C Age of DOC_{photo}	-	Modern*	Modern*	Modern*	Modern	Modern	Modern	Modern	Modern

621 **Table 3 |** Raw and volume corrected counts for irradiated samples, process blanks and ultrapure
622 water blanks based upon flow cytometry.

623

Sample Type	% Permafrost DOC	Counts	Counts per mL*
Permafrost Thaw Stream	100%	2	49
Permafrost/Kolyma Mix	98%	29	711
Permafrost/Kolyma Mix	92%	0	0
Permafrost/Kolyma Mix	66%	6	151
Permafrost/Kolyma Mix	39%	7	173
Permafrost/Kolyma Mix	17%	6	144
Permafrost/Kolyma Mix	3%	3	74
Permafrost/Kolyma Mix	1%	0	0
Kolyma River Mainstem	0%	2	49
Pantileikha River	-	3	73
Y4	-	14	348
Y3	-	206	4951
Sample Blank	-	66	1628
Ultrapure Water Blank	-	10	245

624 *Sample volumes varied from 39.8 to 41.6 μL; the average flow rate was 15.9±4.5 μL min^{-1}.

625

626

Figure captions:

Figure 1: Study site and sample locations. Individual site latitude and longitude are provided in Table 1. Upper right panel is a map centered on the north pole with land in black and sea in grey.

Figure 2: Panels a and b) Bar charts grouping the percentage of photoresistant, photo-labile, and photoproduced molecular formulas by modified aromaticity index. **a:** permafrost thaw water stream. **b:** Kolyma River mainstem. **Panels c and d)** van Krevelen diagrams where each dot represents one molecular formula, and where color indicates the change in normalized signal intensity in mass spectra caused by 30 days of photo-modification in a solar simulator for, **c:** permafrost thaw water stream, and **d:** Kolyma River mainstem. Tables embedded in Panels c and d present the number of total, photoproduced, photo-labile, and photorefractory molecular formulas.

Figure 3: Results from 30 day photochemical irradiations of mixtures of yedoma permafrost thaw stream and Kolyma River mainstem water. **a:** Loss of colored dissolved organic matter (CDOM) light absorption (*a*) at 254 nm. **b:** Percentage photo-labile dissolved organic carbon (DOC). **c:** Percentages of photo-labile molecular formulas. **d:** Fraction modern ($F^{14}C$) for DOC in the mixtures before and after irradiation. Light and dark green regions on a to c indicate the 95% confidence of fit and prediction respectively. Error bars are drawn at 1 standard deviation. d has no error bars as each sample was analyzed only once via ultrahigh resolution Fourier ion cyclotron resonance mass spectrometry.

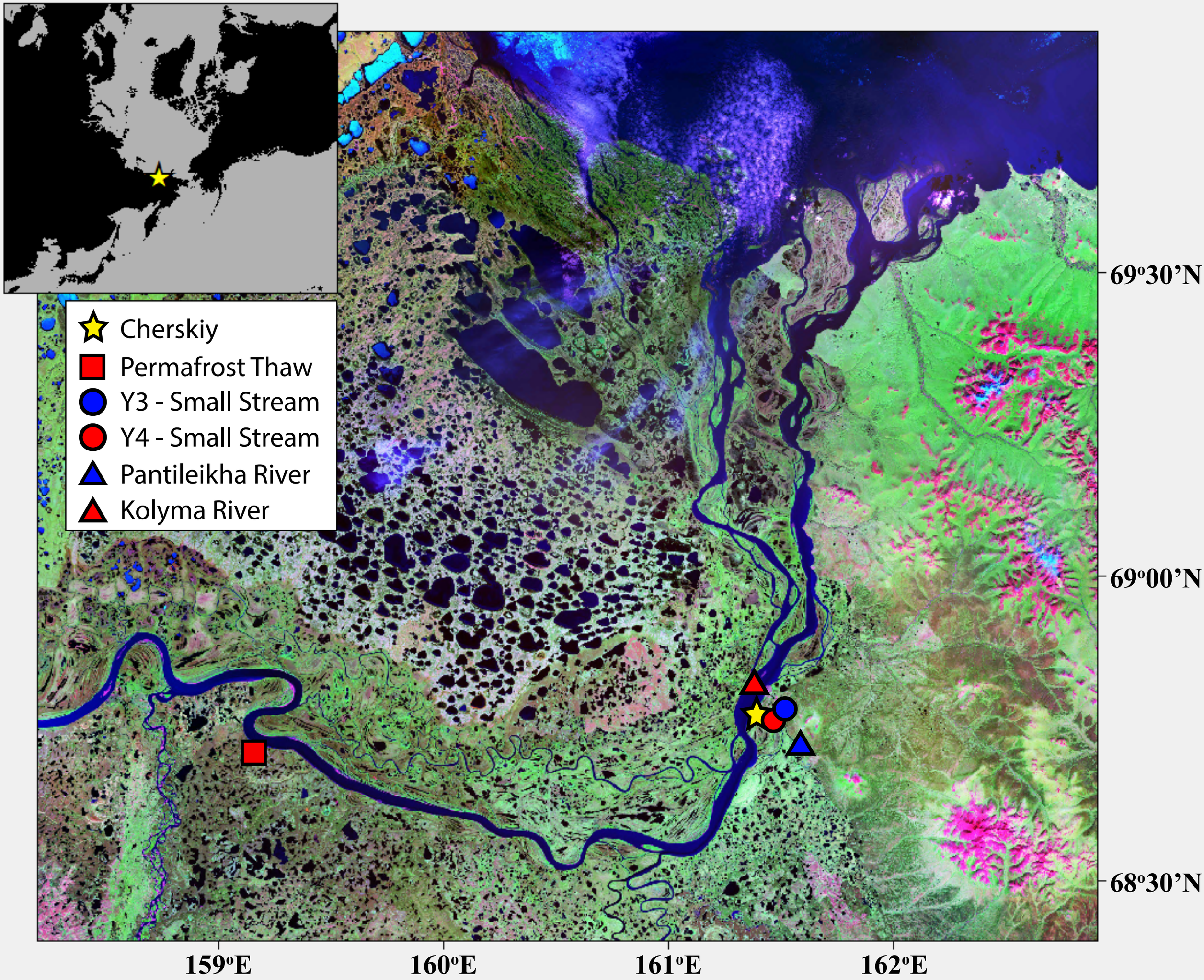

Figure 1: Study site and sample locations. Individual site latitude and longitude are provided in Table 1. Upper right panel is a map centered on the north pole with land in black and sea in grey.

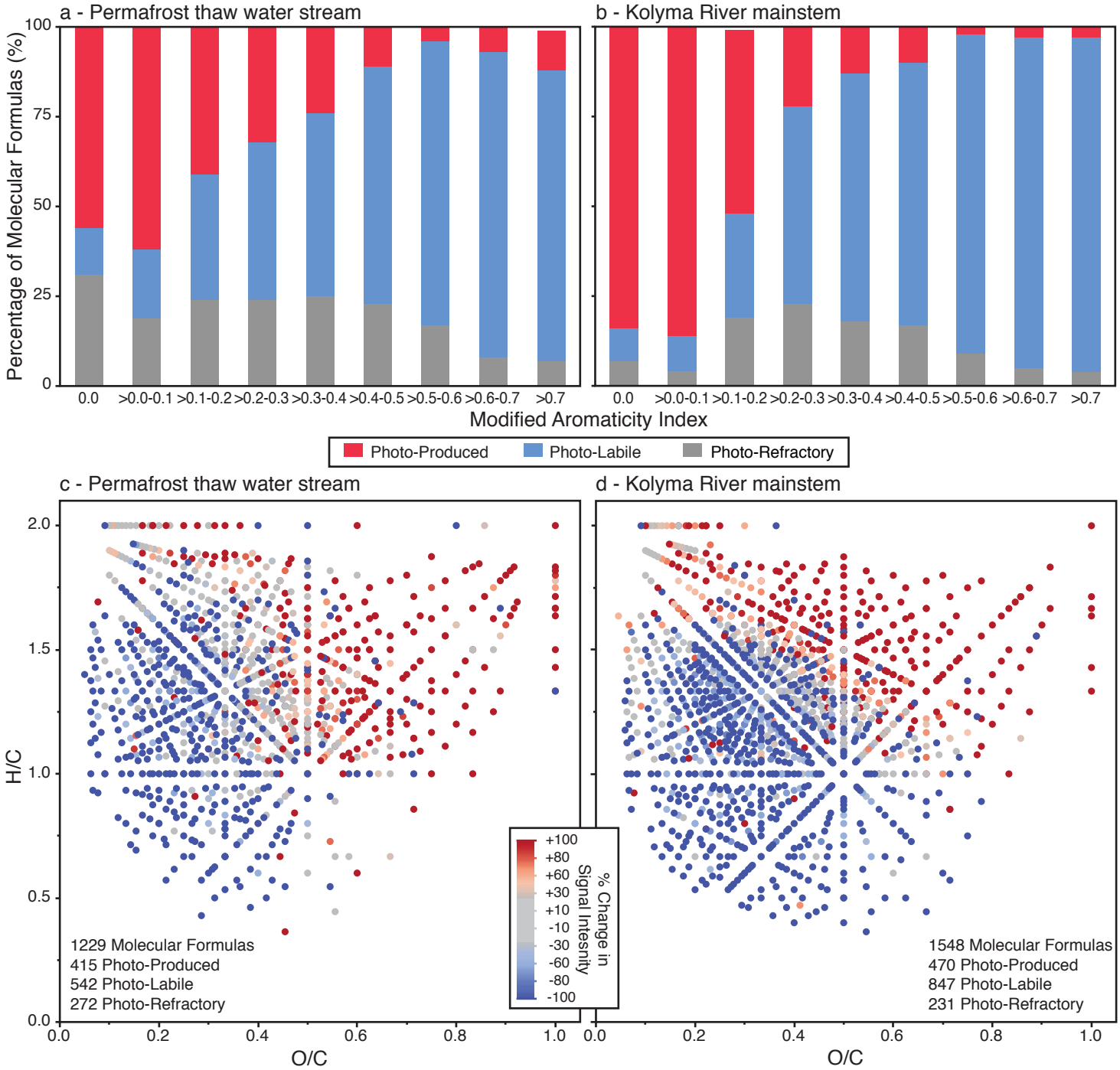

Figure 2 | Panels a and b) Bar charts grouping the percentage of photoresistant, photo-labile, and photoproduced molecular formulas by modified aromaticity index. **a:** permafrost thaw water stream. **b:** Kolyma River mainstem. **Panels c and d)** van Krevelen diagrams where each dot represents one molecular formula, and where color indicates the change in normalized signal intensity in mass spectra caused by 30 days of photo-modification in a solar simulator for, **c:** permafrost thaw water stream, and **d:** Kolyma River mainstem. Tables embedded in **Panels c and d** present the number of total, photoproduced, photo-labile, and photorefractory molecular formulas.

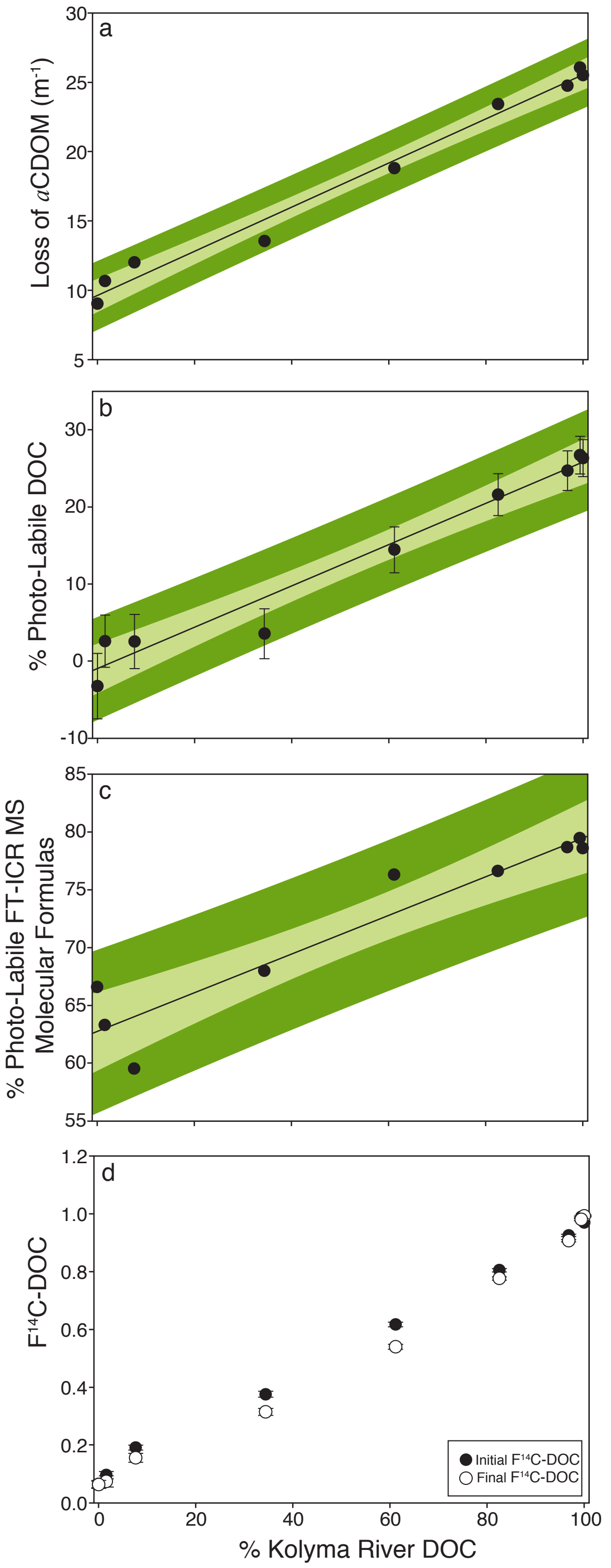

Figure 3 | Results from 30 day photochemical irradiations of mixtures of yedoma permafrost thaw stream and Kolyma River mainstem water. **a)** Loss of colored dissolved organic matter (CDOM) light absorption (*a*) at 254 nm. **b)** Percentage photo-labile dissolved organic carbon (DOC). **c)** Percentages of photo-labile molecular formulas. **d)** Fraction modern ($F^{14}C$) for DOC in the mixtures before and after irradiation.